Arab J Geosci (2016) 9: 322
DOI 10.1007/s12517-016-2329-6

ORIGINAL PAPER

Implementation of integrated multi-channel analysis of surface waves and waveform inversion techniques for seismic hazard estimation

Abd el-aziz Khairy Abd el-aal[1] · Yuji Yagi[2] · Heba Kamal[3] · kamal Abdelrahman[1,4]

Received: 2 August 2014 / Accepted: 20 January 2016 / Published online: 12 April 2016

Abstract In this study, an integrated multi-channel analysis of Surface Waves (MASW) technique is applied to explore the geotechnical parameters of subsurface layers at the Zafarana wind farm. Moreover, a seismic hazard procedure based on the extended deterministic technique is used to estimate the seismic hazard load for the investigated area. The study area includes many active fault systems along the Gulf of Suez that cause many moderate and large earthquakes. Overall, the seismic activity of the area has recently become better understood following the use of new waveform inversion method and software to develop accurate focal mechanism solutions for recent recorded earthquakes around the studied area. These earthquakes resulted in major stress-drops in the Eastern desert and the Gulf of Suez area. These findings have helped to reshape the understanding of the seismotectonic environment of the Gulf of Suez area, which is a perplexing tectonic domain. Based on the collected new information and data, this study uses an extended deterministic approach to re-examine the seismic hazard for the Gulf of Suez region, particularly the wind turbine towers at Zafarana Wind Farm and its vicinity. Alternate seismic source and magnitude-frequency relationships were combined with various indigenous attenuation relationships, adapted within a logic tree formulation, to quantify and project the regional exposure on a set of hazard maps. We select two desired exceedance probabilities (10 and 20 %) that any of the applied scenarios may exceed the largest median ground acceleration. The ground motion was calculated at 50th, 84th percentile levels for both selected probabilities of exceeding the median.

Keywords MASW · Waveform inversion · Seismic hazard · Wind turbine towers · Zafarana wind farm

✉ Abd el-aziz Khairy Abd el-aal
dewaky@yahoo.com

[1] Seismology Department, National Research Institute of Astronomy and Geophysics, Cairo, Egypt

[2] Faculty of Life and Environmental Sciences, University of Tsukuba, Tsukuba, Japan

[3] Housing & Building National Research Centre (HBRC), Cairo, Egypt

[4] Geology and Geophysics Department, College of Science, King Saud University, Riyadh, Saudi Arabia

Introduction

The need to diversify the global energy portfolio to meet increasing energy demands while reducing reliance on fossil fuels has led to a significant development of renewable sources of energy in recent decades, especially wind energy. Wind turbine technology has developed tremendously over the past few years. As such, wind energy plays a pivotal role in satisfying the increasing energy demands in the country. The Zafarana wind farm is an area of about 80 km^2 earmarked by the New and Renewable Energy Authority to implement large-scale grid connected wind farms. This wind farm project has been implemented in several stages starting in 2001, through governmental cooperation protocols with Germany, Denmark, Spain and Japan as shown in Fig. 1. The Zafarana Wind Farm is located 120 km south of Suez on the Red Sea in the Zafarana area (Fig. 1). Zafarana wind farm is currently generating a capacity of 517 MW, making it one of the largest onshore wind farms in the world. More details about Zafarana wind farm can be found in Abd el-aal et al. (2015).

The waveform inversion technique is considered a valuable and important means of obtain moment tensor solutions, from which it is possible to obtain the faulting type of an earthquake, the moment magnitude (Mw) and seismic moment (Mo). The

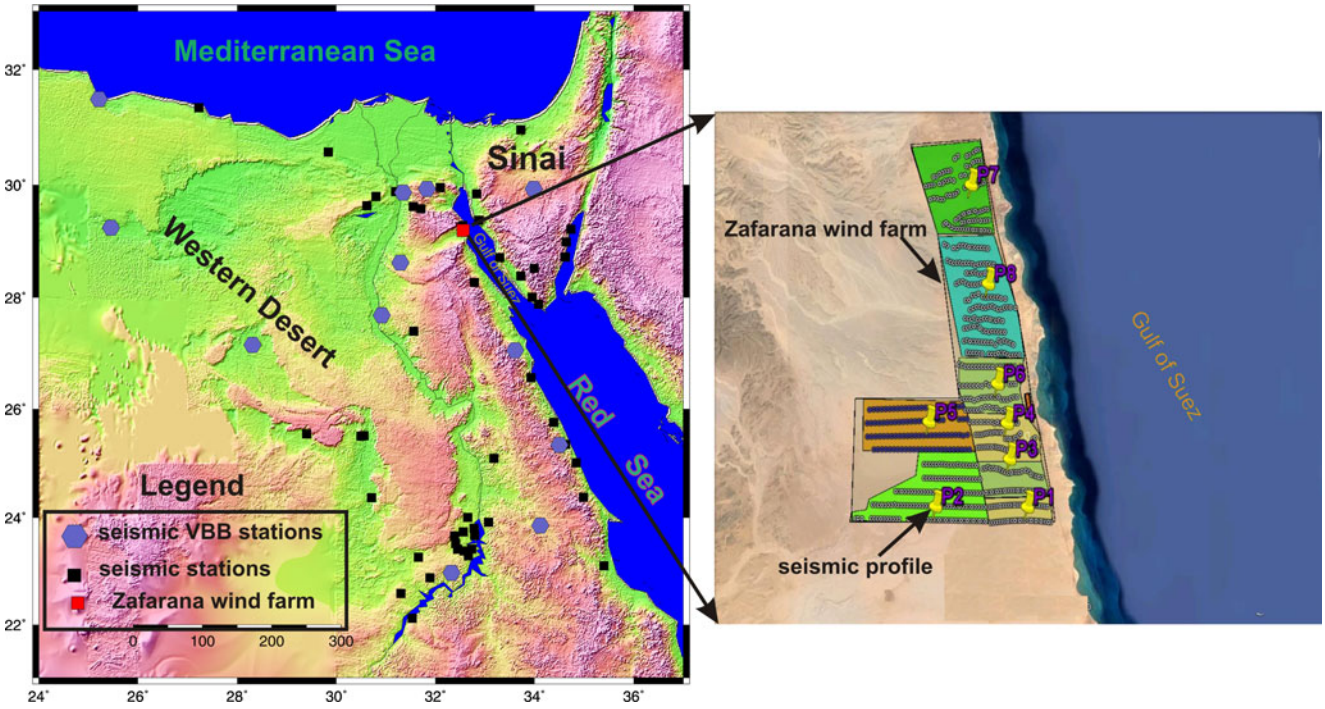

Fig 1 Location map of Zafarana Wind Farm and the Egyptian National Seismological Network includes both very broadband stations (purple hexagonal) and short period and broadband station. Right panel is the satellite image of Zafarana Wind Farm shows the location of conducted seismic lines

seismic source process for any earthquake mainly depends on information obtained by waveform inversion and moment tensor solutions (Abd el-all and Yagi 2015, Moment tensor solutions, earthquake source parameters and stress field for moderate earthquakes occurred in northern Red Sea triple junction by waveform inversion, under review; Yagi and Nishimura 2011, Yagi and Fukahata 2012; Yagi et al. 2012).

Near surface geophysical surveys such as multi-channel analysis of surface waves (MASW) and shallow seismic refraction have been widely applied in civil engineering; i.e. in road tunnelling, dam sites, wind farms, quarries, hydroelectric power plants, subway constructions, nuclear power plants, cavity and fault detection and many other purposes. P- and S- wave velocity measurements, obtained using both the MASW technique and shallow seismic refraction surveys, are used to evaluate the bedrock in order to determine the elastic properties of the materials in the sites under assessment. The SH (horizontal shear) waves can be used to study the vibration characteristics of the subsurface layers, which are important for earthquake resistant structural design. The estimation of the effects of near-surface geology on seismic motion is a critical component of seismological research, since it is necessary to separate site effects from the source and path effects in order to interpret the nature of the ground motion. Such near surface geology plays an important role in earthquake hazard analysis. In particular, it is well-known that thick soil sites are subject to increased ground motion in comparison to rocky sites (e.g. Aki, 1993). Also, younger and softer soils amplify ground motion more strongly than older and more compacted soils (Montalvo-Arrieta et al., 2002).

In its common form, deterministic seismic hazard analysis (DSHA) detects the seismic source or sources that may have an impact on the investigated site and then assesses the maximum possible earthquake magnitude for each of these seismic sources. By assuming that each of these maximum earthquakes occurs at a location that places the earthquake at the minimum possible distance to the site of interest, then the ground motion is predicted, mostly utilizing an empirical attenuation relation. The DSHA approach estimates ground motions (for the mean and specified fractiles of the ground motion dispersion) corresponding to the largest magnitude occurring at each seismic source at its closest approach to the site of interest. These results can be applied to various types of structural analyses. In general, buildings in Egypt are not designed to resist earthquakes; therefore relatively small events can result in huge socio-economic disasters (Abd el-aal 2010a). Protection of strategic structures like nuclear power plants, dams and highly-populated areas from all kinds of hazards, particularly earthquakes, is the essential mission of seismologists and civil engineers in Egypt for now and the foreseeable future (Abd el-aal 2008; Abd el-aal 2010b).

Aim of study

The Zafarana wind farm is located in an active seismic zone along the west side of the Gulf of Suez. Accordingly, seismic

hazard and seismic risk assessment are necessary in order to assess the structural integrity of wind towers under expected seismic hazard events. The current Egyptian design codes lack provisions for either aerodynamic or seismic design loadings for wind turbine towers. The current seismological studies, dynamic field measurements and structural seismic analyses of existing wind towers, will greatly enhance the associated design recommendations. For instance, the actual estimated site loads can be applied to any new towers constructed in the same zone or in new zones in the future. The field seismic measurements and new wind turbine ambient vibration datasets that will be acquired through this research at Zafarana will also constitute a basis for calibration of analysis tools. This data will be professionally archived and made available for use by interested researchers and practitioners worldwide. Valuable recommendations will be deduced for provisions in design codes based on realistic data and detailed structural assessments of the wind turbines.

Another aim of this paper is a pilot near-surface characterization and its effect on seismic hazard estimation using integrated and new techniques at Zafarana Wind Farm. Multi-channel analysis of Surface Waves (MASW) will be used to provide information on the near-surface velocity structure in order to identify major acoustic impedances within the overburden, and to delineate any local subsurface structure. This study demonstrates the applicability of near-surface seismic techniques to such site characterizations for deriving strong-motion prediction equations. The results of this study will be of relevance to similar studies in the Middle East at large, as well as in other seismically active regions of the world.

Seismotectonic, seismicity, seismic sources and subsurface geology

Tectonically speaking, Egypt is located at the northeast corner of Africa and is bounded by three active tectonic margins: the African-Eurasian plate margin; the Red Sea plate margin; the Levant-Dead Sea transform fault (Fig. 2). There are three main tectonic deformations affecting northern Egypt: Jurassic-Early Cretaceous rifting, Late Cretaceous-Early Tertiary wrenching and Miocene and post-Miocene extension. The detailed subsurface and surface studies that have been carried out in northern Egypt indicate that the Miocene and post-Miocene extension in this region is due to the rift of Arabia away from Africa, which has formed a large number of NW-SE oriented normal faults and rejuvenated the E-ENE oriented faults in the Cairo-Suez district by dextral transtension (Moustafa et al., 1998). Due to the Suez rift being unable to extend north of Suez City, the throw on the faults in the northern part of this Miocene rift was transferred into the Cairo-Suez district (Moustafa and Abd-Allah, 1992). This throw was transferred through the deep-seated EW oriented faults and led to their rejuvenation by dextral transextension to form EW elongated belts of left-stepped en-echelon normal faults in addition to NW-SE oriented normal faults (Fig. 3). The transfer of the throw continues northwestward toward the area west of the Nile Delta (Moustafa et al., 1998). The EW faults (oblique-slip movement with a subordinate right-lateral strike slip component) are generally linked at depth to the NW-SE faults (pure dip-slip) and act as a transfer zone.

Low to moderate seismic activity is clustered in and around the studied area and also in the Gulf of Suez and its extension (Fig. 3). Significant seismic activity is also found along the entire Gulf of Suez and its extension in the northern part of the Egyptian Eastern Desert toward the Nile Delta along the E-W and WNW faults. The seismic activity in the Gulf of Suez is scattered, however, and does not have any distinct trend at the present time. Three active zones are delineated along the Gulf of Suez. At the mouth of the gulf most activity is concentrated where the Sinai triple junction (Africa, Arabia, and Sinai) is situated. The central part and the northern part of the gulf include the adjacent area as far as the river Nile. Actually, the activity is markedly decreased from south to north. Although there is no seismological evidence that the Suez rift continues into the eastern Mediterranean, the activity in the Gulf of Suez region cannot be ignored.

Historically, some events have been reported inside the Gulf of Suez (i.e. the event of July 11, 1879 (MF = 5.9, Ambraseys et al., 1994). Moreover, the destructive earthquake which took place at the apex of the Suez Gulf at October, 1754 with intensity ranges ~VII-IX and MF of 6.6 (Ambraseys et al., 1994) and the Shadwan earthquakes of 600BC and 27/28BC may have had a large effect. (Maamoun et al., 1984). All the historical events have been compiled from available local and international sources (Poirier and Taher, 1980, Maamoun et al., 1984, Ambraseys et al., 1994).

Instrumental seismicity from 1900 to Aug., 2013 is clustered in the northern Red Sea and extends north along the Gulf of Suez (Figs. 2 and 3). Moreover, many small-moderate sized events, with magnitudes up to ML = 5, have been reported inland along the Suez-Cairo shear zone (Abd el-aal 2010a, 2010b). The majority of these activities overlie a well-defined fault NW-SE along the borders of the Gulf of Suez and EW to WNW surface faults inland. Based on geological, structural, seismic activity and focal mechanisms, Abd el-aal et al. (2015) specified the seismic sources in the Gulf of Suez and its surroundings (Fig. 2). The seismicity parameters of these sources are evaluated based on the recent seismicity from 1900 up to 2013.

Abd el-aal et al. (2015) indicated that the subsurface geological features in the Zafarana project area consist of coastal and wadi deposits (Fig. 4). There are no intensive faults in the Zafarana area. Based on the results of the previous site investigation and laboratory testing, the subsurface

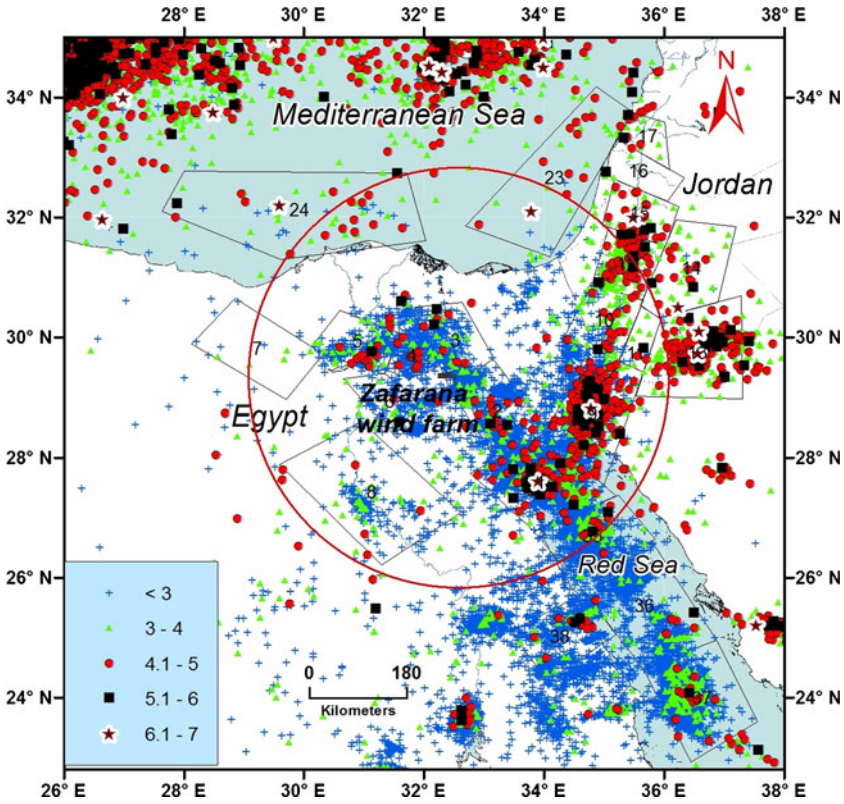

Fig 2 Seismicity map of Egypt. The unified catalogue Mw of earthquakes from 1900 to 2013 used in this study. Red circle with radius 300 km is plotted around the studied area. The map shows delineated seismic sources within 300 km in and around Zafarana wind Farm site, Gulf of Suez. The map also illustrates the developed seismotectonic model used to estimate seismic hazard at Zafarana Wind farm site. 38 seismic sources were identified

formation consists of wadi deposits, sand, sandstone and claystone. More details about subsurface geology at Zafarana wind farm can be found in Abd el-aal et al. (2015).

Applied techniques

Waveform inversion technique and source parameters

This paper presents a waveform inversion and source mechanism study of the three largest seismic events that have occurred near the Zafarana wind farm since 2010. The source process and focal mechanisms for those events have been calculated with a new seismic moment tensor inversion method using new software (Abd el-all and Yagi 2015, Moment tensor solutions, earthquake source parameters and stress field for moderate earthquakes occurred in northern Red Sea triple junction by waveform inversion, under review; Yagi and Nishimura 2011). Seismic moment tensor solutions and the physical parameters of seismic events in and around the investigated area can provide very useful information for accurate hazard estimation. The information about focal mechanisms and source parameters can be used in hazard assessment together with the focal coordinates of earthquakes.

Since 2009, the dramatic increase in the deployment of broadband and very broadband seismic stations with real-time continuous telemetry has meant that moment tensor determination has become increasingly feasible in Egypt, and moment tensor solutions are now a very important product of the Egyptian National Seismic Network (ENSN) (Abd el-aal 2013; Abd el-aal and Soliman 2013).

We used a new method and software package for moment tensor solution and waveform inversion. The new method and software used in this study treat the effect of the source time function, which have been neglected in most previous programme sets for moment tensor inversion analysis with near source seismograms. The method is suitable for middle-sized earthquakes because the occurrence rate of middle-sizes earthquake is higher than that of large-size earthquakes, which assists in the estimation of stress field and faulting systems in local regions (Abd el-all and Yagi 2015, Moment tensor solutions, earthquake source parameters and stress field for moderate earthquakes occurred in northern Red Sea triple junction by waveform inversion, under review; Yagi and Nishimura 2011; Yagi and Fukahata 2012).

The following is a summary of the method; for more details refer to Abd el-all and Yagi 2015, Moment tensor solutions, earthquake source parameters and stress field for moderate earthquakes occurred in northern Red Sea triple

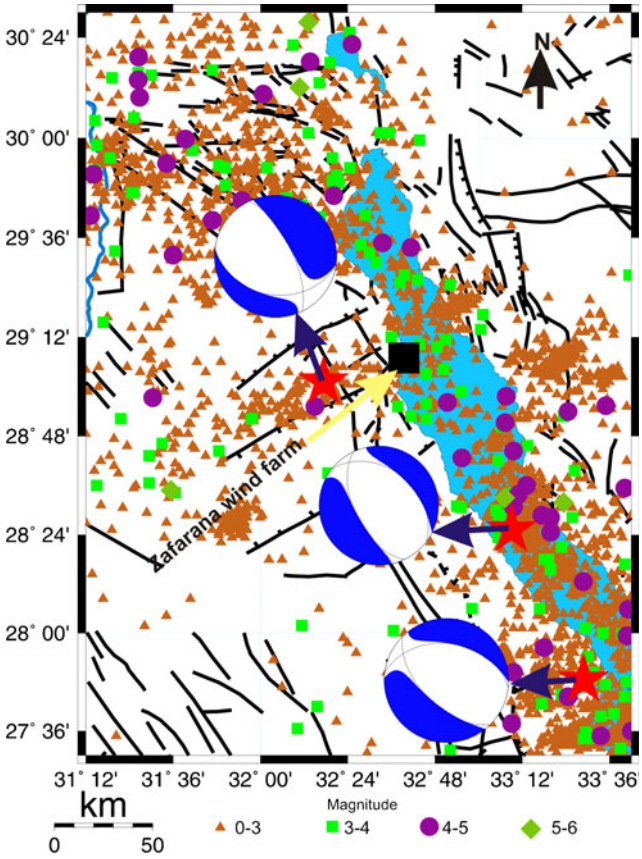

Fig 3 Seismicity map of the Gulf of Suez and its vicinity. The focal mechanism and fault plane solutions of largest three studied earthquakes occurred near the investigated area are also plotted

junction by waveform inversion, under review and Yagi and Nishimura (2011). The observed waveform (u) of component (c) (eg. velocity, acceleration and displacement) can be expressed as:

$$u_c(x,t) = G*M \tag{1}$$

Where the term G is the Green's functions, representing all propagation effects of the medium on elastic waves, while M is the seismic moment release, represented by the scalars M_{kj} with the unit of a moment of force. Additional external forces are neglected. This symmetric 3 × 3-tensor contains six independent elements:

$$M_{kj} = \begin{pmatrix} M_{xx} & M_{xy} & M_{xz} \\ M_{yx} & M_{yy} & M_{yz} \\ M_{zx} & M_{zy} & M_{zz} \end{pmatrix} \tag{2}$$

The symmetry of the tensor yields a total moment of forces of zero. This leads to the model of the double couple: the two elements, M_{yz} and M_{zy}, build a double couple that leads to a pure shear failure when the stress in the material exceeds a critical mechanic threshold.

Eq. 1 can be written in detail as follows:

$$u_c(x,t) = \sum_{q=1}^{6} \iiint_v G_{xcq}(t,\xi) * M_q(t,\xi) d\xi + e_{xc}(t), \tag{3}$$

Where e is the observed error. Since the volume change during an earthquake is too small to detect, the volume change component, M_6, is neglected. A simple source model such as a point source, in which the seismic waveforms radiate from one point, is also assumed, which leads to eq.3 being rewritten as follows:

$$u_c(x,t) = \sum_{q=1}^{5} G_{xcq}(t,\xi_c) * M_q(t) + e_{xc}(t), \tag{4}$$

Where ξ_c is the location of the centroid. It was also assumed that the focal mechanism remains constant during the earthquake and that the shape of the source time function could be approximated to be an isosceles triangle with a half duration of t_r. This allows eq. 4 to be written as follows:

$$u_c(x,t) = \sum_{q=1}^{5} G_{xcq}(t,t_r,\xi_c) \times M_q(t) + e_{xc}(t), \tag{5}$$

After applying the low-pass filter to the observed data, an N –dimensional data matrix is obtained. The solution of the matrix equation is obtained by the least squares approach. Yagi and Nishimura (2011) assumed that the horizontal location of the centroid can be approximated to the epicentre of the earthquake and that it is therefore possible to estimate the optimal depth of the centroid and half duration using the grid-search method. Fig.1 shows the very broadband stations used in this study. For the complete procedure of waveform inversion for earthquakes recorded by the ENSN Network please refer to Abd el-all and Yagi 2015, Moment tensor solutions, earthquake source parameters and stress field for moderate earthquakes occurred in northern Red Sea triple junction by waveform inversion, under review.

Figure 5 illustrates the observed and synthetic waveforms and corresponding obtained moment tensor solutions for two of the analysed events. The obtained fault plane solutions of the respective earthquakes exhibited normal faulting mechanisms (Fig 3). For these analysed events, Table 1 lists the possible range of the mechanisms in strike, dip, rake tensor elements and moment.

The source parameters, such as the fault radius (r_0), the stress drop ($\Delta\sigma$), rupture area and dislocation were determined for the three studied main shocks that occurred recently (March 25, 2013, Mw = 3.8; April 11, 2013 Mw =3.2; June 01, 2013 Mw =4.3. A MATLAB code was written to estimate these parameters using the seismic moment obtained by the

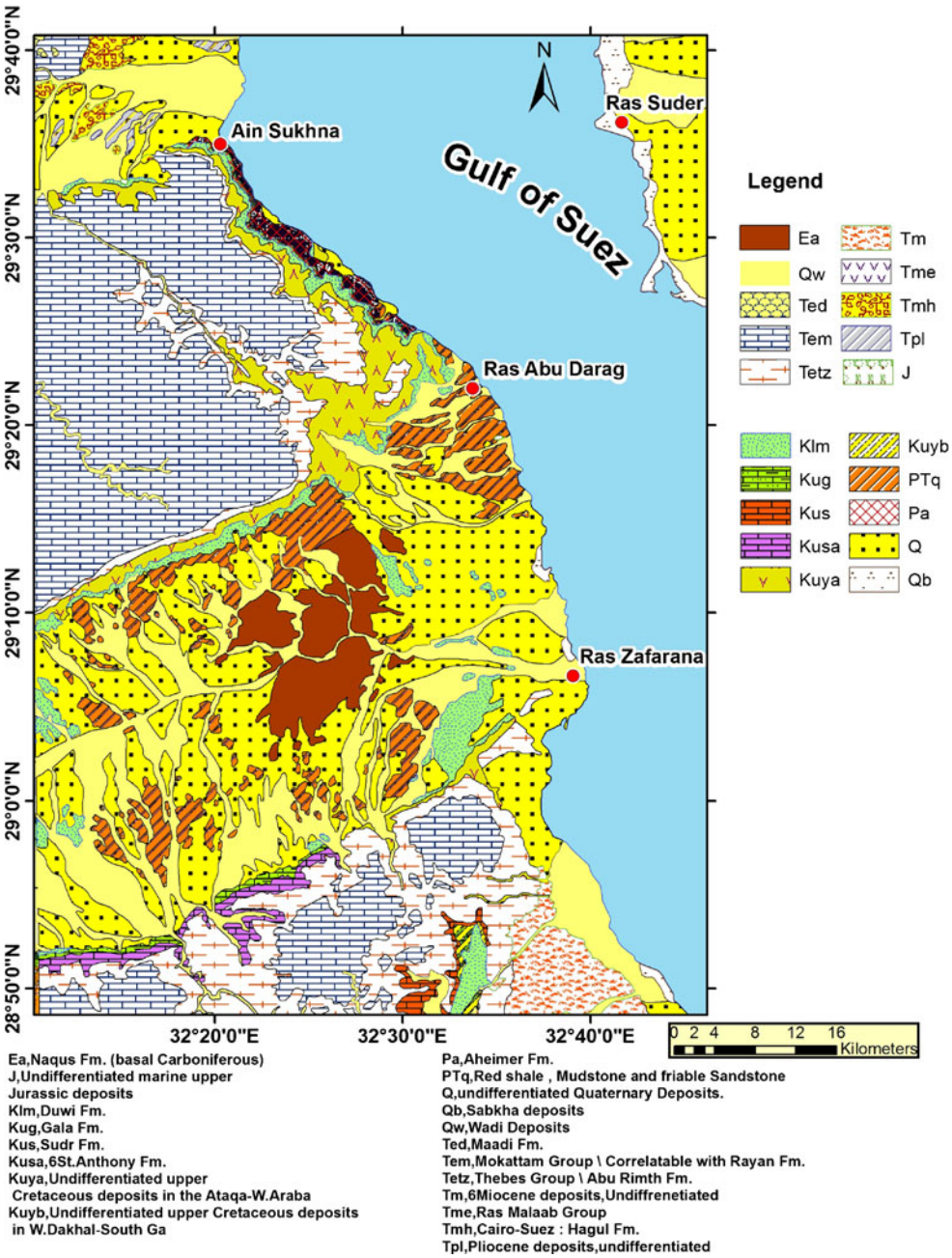

Fig 4 Surface geology map of the Zafarana Wind Farm site and its surrounding. The map shows the lithological unites cover the area (after EGSMA, 1983)

inversion technique. Using the Hanks and Wyss (1972) relations we obtained:

$$r_0 = \frac{2.34(vp)}{2\pi f_o} \tag{6}$$

$$\Delta\sigma = \frac{7M_0}{16(r_o)^3} \tag{7}$$

Where vp is the P-wave velocity, f_o is the corner frequency and M_0 is the seismic moment. In the present work, in order to estimate the maximum magnitude Mmax for each seismic event for the determined faults, we used the relationships in Hanks and Bakun (2002).

$$\text{Mmax} = \log A + 3.98 \quad A \leq 557\ \text{Km}^2 \tag{8}$$

Where A is the total ruptured area that can be calculated by the relationship of Fukao and Kikuchi (1987):

$$A = \pi(V_r t/2)^2 \tag{9}$$

Where $V_r$is the rupture velocity (typically V_r is in the range 0.7–0.9v_s, being v_s the shear wave velocity), t

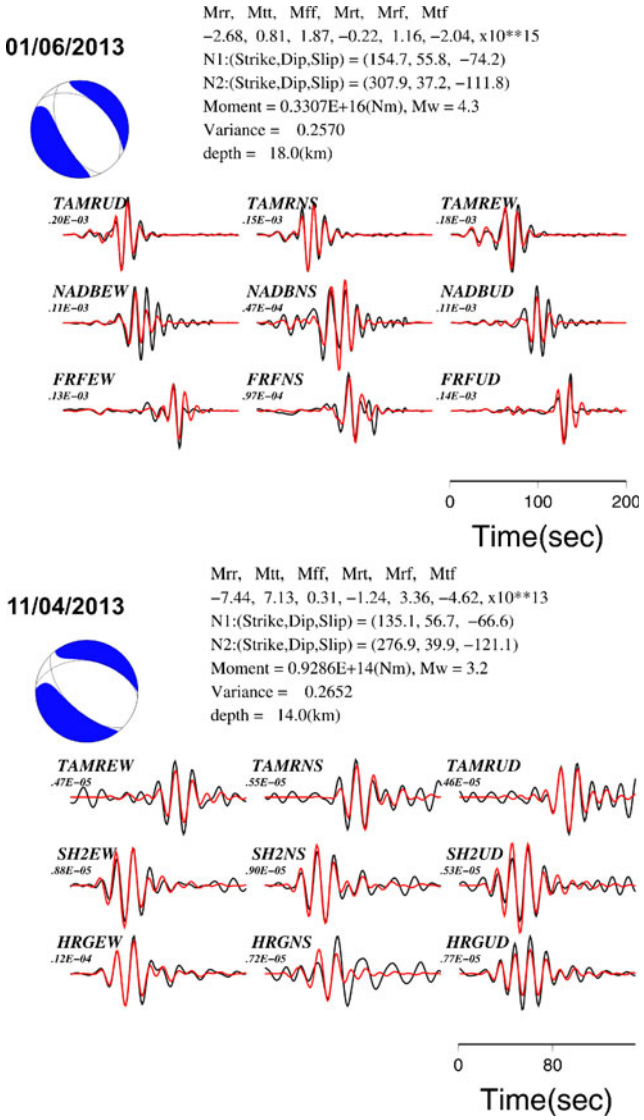

Fig 5 Examples of inversion result, with comparison of the synthetic data with the observed data (black line represents observed data, red line represents the synthetic waveform), (upper panel) june.1, 2013; (lower panel) April 11, 2013

represents the rupture duration. The term $V_r t/2$ represents the fault radius (r_0). Table 2 shows the instrumental data on the studied earthquakes, their source parameters and the expected Mmax from the assigned faults around the investigated area.

Multi-channel analysis of surface waves (MASW)

Recently, the multichannel analysis of surface waves (MASW) has been considered to be one of the most practical non-invasive seismic exploration methods for use in engineering seismology. In comparison to conventional seismic tests, it is less expensive and has the benefit of precision and swiftness in estimating the subsurface shear wave velocity profile over a

Table 1 Fault plane solution and moment tensor elements for studied earthquakes as deduced from waveform inversion

no	Date (d/m/y)	Time (h:m)	Lat. (N)	Long. (E)	Depth (km)	strike (N1)	dip (N1)	rake (N1)	Mrr	Mtt	Mff	Mrt	Mrf	Mtf	Exponent (Nm)
1	25/03/2013	12:40	29.0234	32.2930	20	97.7	36.8	−140.8	−3.50	2.67	0.83	0.87	−3.57	−3.49	1.00E + 14
2	11/04/2013	3:56	27.8088	33.4812	14	135	56.7	−66.6	−7.44	7.13	0.31	−1.24	3.36	−4.62	1.00E + 13
3	01/06/2013	11:49	28.4178	33.1506	18	154.7	55.8	−74	−2.68	0.81	1.87	−0.22	1.16	−2.04	1.00E + 15

Table 2 The studied instrumental earthquakes and its source parameters as induced from waveform inversion technique

no	Effective studied earthquakes								Maximum Expected magnitude Mmax	Distance to study area (Km)
	Date (d/m/y)	Coordinates		Source parameters						
		Lat	Long	$\Delta\sigma$ (bar)	M_0 (Nm)	Magnitude M_w	r_0 (km)	Rupture Area (km^2)		
1	25/03/2013 (Ml = 4.2)	29.0234	32.2930	1.87	0.594×10^{15}	3.8	1.12	3.92	4.6	32
2	11/04/2013 (Md = 3.5)	27.8088	33.4812	0.36	0.928×10^{14}	3.2	1.03	3.36	4.5	162
3	01/06/2013 (Mb = 4.8)	28.4178	33.1506	0.66	0.331×10^{16}	4.3	2.79	24.5	5.4	95

large area (Park et al., 1999). The shallow seismic techniques for near-surface investigation have usually been either high-resolution refraction or reflection surveys that deal with a sub-surface depth range from a few tens to hundreds metres. The seismic signals from these surveys consist of wavelets with frequencies higher than 50 Hz. On the other hand, the multi-channel analysis of surface waves (MASW) method deals with surface waves in the lower frequencies (e.g., 1–30 Hz) and uses a much shallower depth range of investigation (e.g., a few to a few tens of metres).

Dispersion, or change in phase velocity with frequency, is the fundamental property utilized in surface wave methods. Shear wave velocity can be derived by inverting the dispersive phase velocity of surface waves. The phenomena of surface wave dispersion can be observed in the presence of velocity layering, which is common in the near-surface environment (the upper 100 m). In this application, we are concerned with the Rayleigh wave, also known as "ground roll". In surface wave methods, the surface waves are generated in two ways. The first one is "Active source", meaning that the seismic energy is intentionally generated at a specific location and recording begins when the source energy is imparted into the ground. The second one is "passive source" where there is no time break and motion from passive, ambient, energy generated by cultural noise, traffic, factories, wind, wave motion, etc. is recorded. It is known that the surface wave energy decays exponentially with depth beneath the surface. The amplitude of any particular frequency is dependent on the ratio of depth to wavelength. Thus, for each frequency, the amplitude decreases by the same factor when the depth increases by a wavelength. This means that the longer wavelength (longer-period, lower frequency) surface waves travel deeper and thus

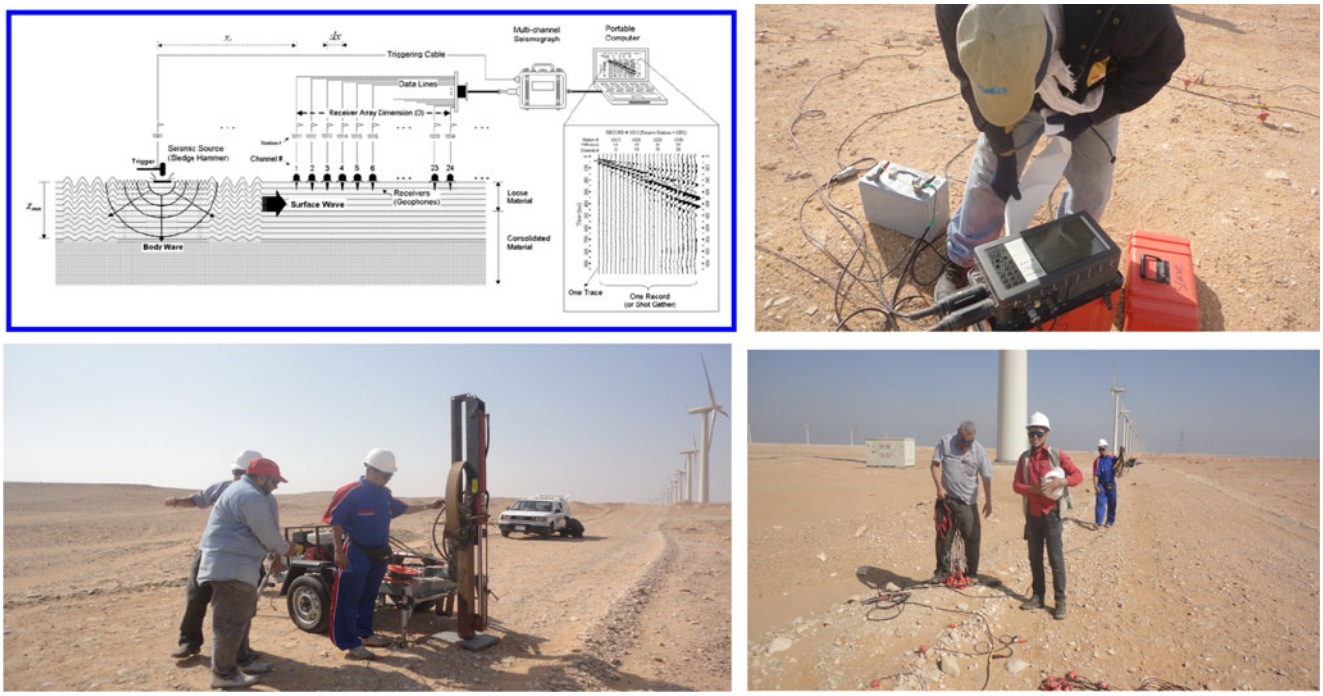

Fig 6 The left upper panel is the MASW (Multi channel Analysis of Surface Wave) data acquisition configuration for determining shear wave velocities. The right upper panel is the StrataView data logger which used in the seismic survey. The left lower panel is the weight drop 150 kg used as source to generate seismic waves. The right lower panel shows geophones and seismic spread design

contain more information about deeper velocity structures, while shorter wavelength (shorter-period, higher-frequency) surface waves travel shallower and thus contain more information about shallower velocity structures. For this reason, the active source surface waves resolve the shallower velocity structures and passive source surface waves sample the deeper velocity structures. The overall setup, field procedures and data processing steps necessary for the method are illustrated in Fig. 6. The maximum depth of investigation (Zmax) that can be achieved is usually in the range of 10–30 m in an active source procedure, but this can vary with sites and the types of active sources used.

The following is a brief mathematical description of the standard method. The first step of the method to calculate the phase difference between two waves $f(t)$ and $g(t)$ in the frequency domain is as follows:

$$F(\omega) = \frac{1}{2\pi} \int_{-\infty}^{\infty} f(t) e^{-i\omega t} dt \tag{10}$$

$$G(\omega) = \frac{1}{2\pi} \int_{-\infty}^{\infty} g(t) e^{-i\omega t} dt \tag{11}$$

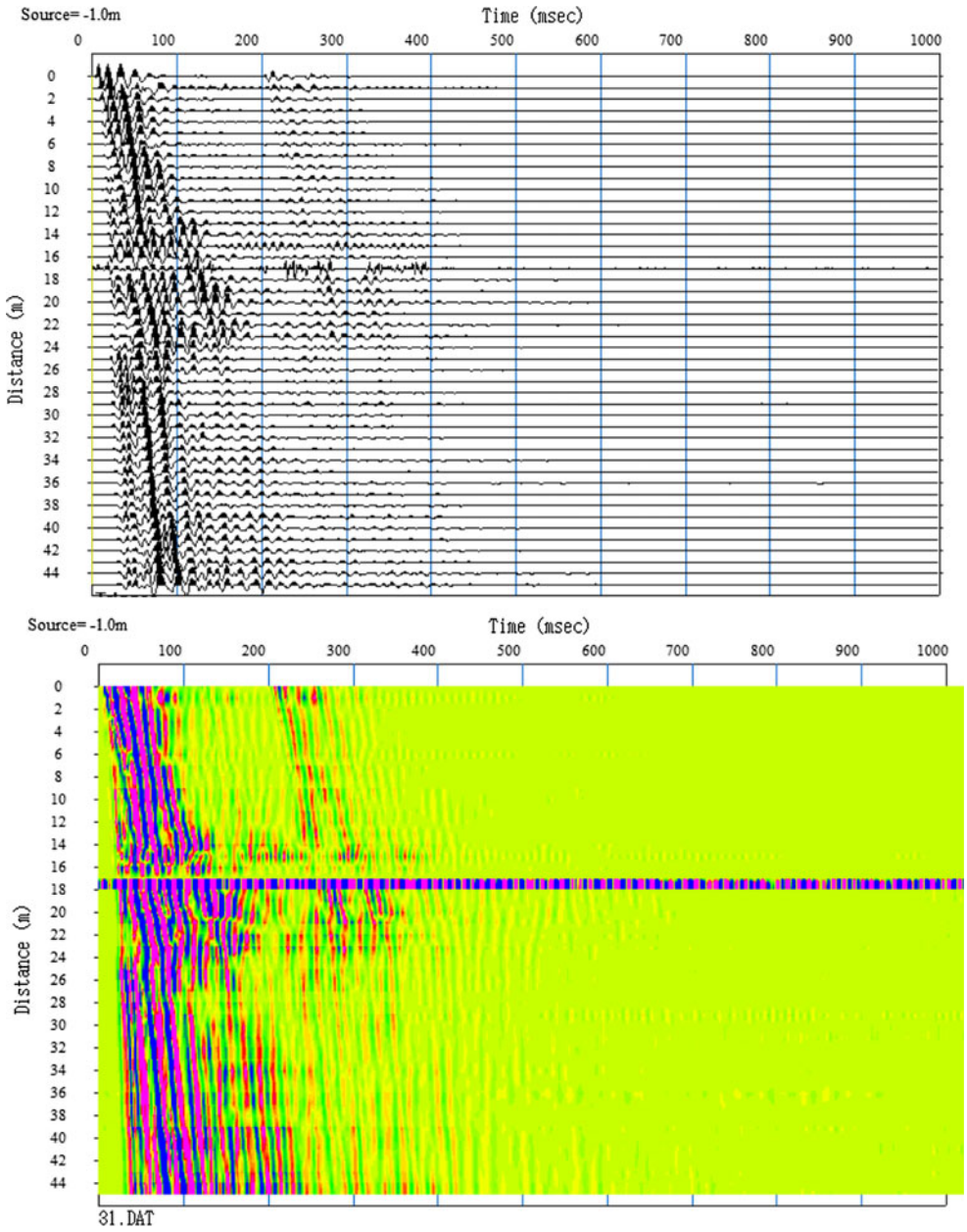

Fig 7 Surface wave data examples as deduced from Multi channel Analysis of Surface Wave technique at seismic line 6 (P6). Please see Fig 1 to see location of the seismic line at the investigated site

Where $f(t)$ and $g(t)$ are the time series data of two waves, respectively, and (ω) is the angular frequency. The amplitude and phase of the two waves can be written as:

$$F(\omega) = A_f(\omega)e^{-i\varphi_f(\omega)} \tag{12}$$

$$F(\omega) = A_g(\omega)e^{-i\varphi_g(\omega)} \tag{13}$$

The phase difference between the two waves can be calculated as follows:

$$\Delta\varphi(\omega) = \varphi_f(\omega) - \varphi_g(\omega) \tag{14}$$

Then, the phase velocity can be calculated as follows:

$$c(\omega) = \frac{\omega\Delta x}{\Delta\varphi_f(\omega)} \tag{15}$$

The next step is creating a semblance that shows the contour of correlation coefficients for selected frequencies and

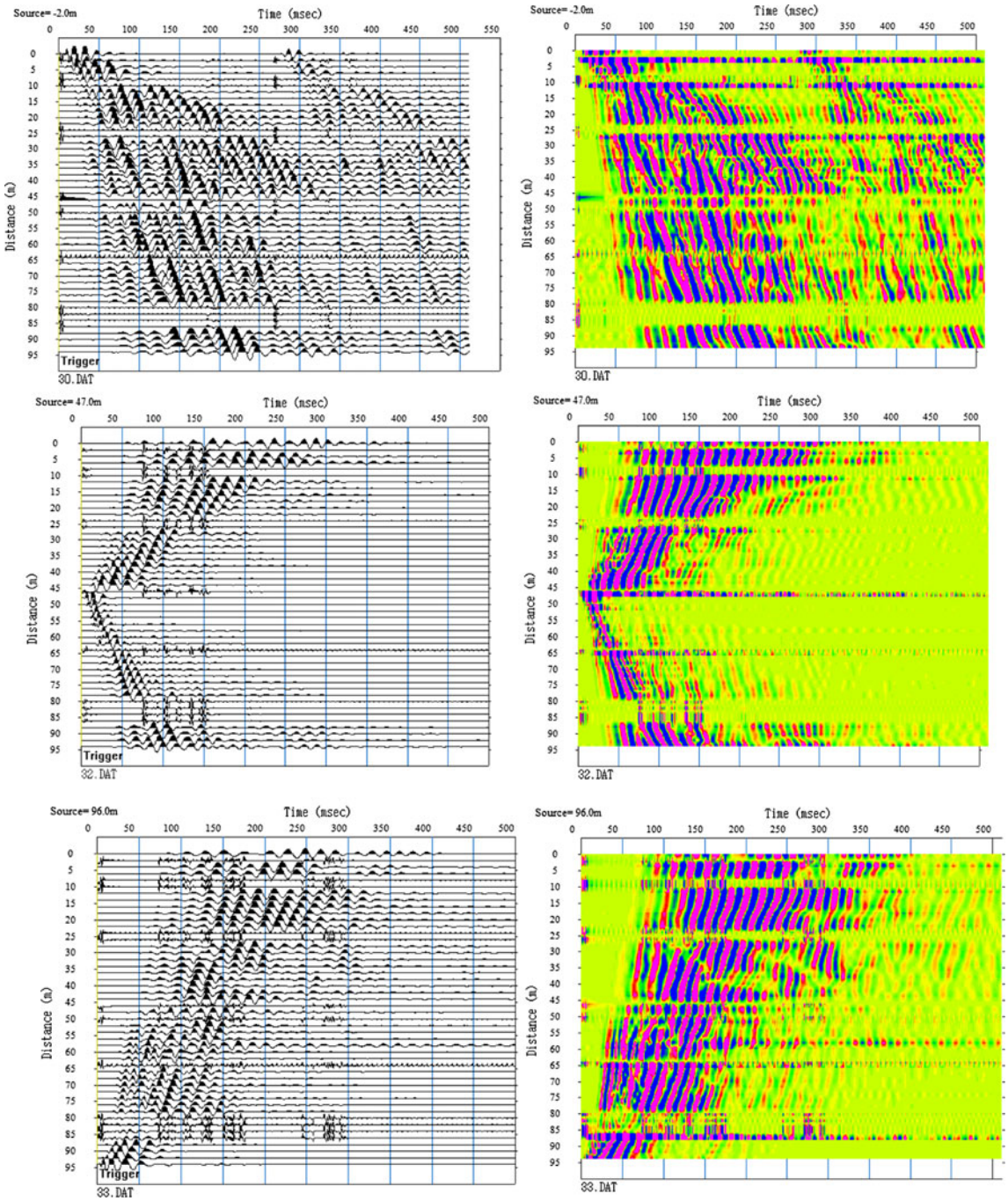

Fig 8 Examples of Seismograms of P- wave data from conducted shallow seismic refraction survey at the investigated site. Both the MASW and shallow seismic refraction lines carried out at the same positions

phase velocities.

$$CC_{fg}(\omega) = F(\omega)\overline{G(\omega)} = A_f(\omega)A_g(\omega)e^{i\Delta\varphi(\omega)} \quad (16)$$

It is important to know the geometry/position of each geophone in order to clarify the correlation variable for several phase velocities, and the phase shift and stacking should be applied to all the traces to get $F(x,\omega)$data. Then, the data is transferred to the semblance using eq. no (17).

$$F(c,\omega) = \int_{-\infty}^{\infty} F(x,\omega)e^{-i\omega\frac{x}{c}}dx \quad (17)$$

Where $F(c,\omega)$ is the group velocities contour versus frequencies. The dispersion curve can then be defined by picking the best correlation from the semblance, i.e. that which shows the best phase velocity for the selected frequency.

The dispersive characteristics of Rayleigh type surface waves were utilized for imaging the shallow subsurface at Zafarana wind farm. In this study, an integrated MASW technique is used here to determine the shear wave velocities in the investigated area. This is the most common type of MASW (Multi channel analysis of surface waves) survey, which can produce a 2-D Vs profile. Eight MASW profiles were carried out at Zafarana wind farm. A 150 kg weight drop was used as a source of active MASW. Vertical stacking with multiple impacts can suppress ambient noise significantly and is therefore always recommended, especially if the survey takes place in an urban area. Low-frequency (4.5 Hz) geophones were used. The length of the receiver spread (D) (Fig. 6) is directly related to the longest wavelength (λ) that can be analysed, which in turn determines the maximum depth of investigation (Zmax): On the other hand, the minimum (if uneven) receiver spacing (dx) is related to the shortest wavelength (λ) and therefore the shallowest resolvable depth of investigation (Zmin). A one millisecond sampling interval is most common with a 2-s total recording time ($T = 2$ s). Figure (7) shows an example of a MASW seismogram conducted at the Zafarana

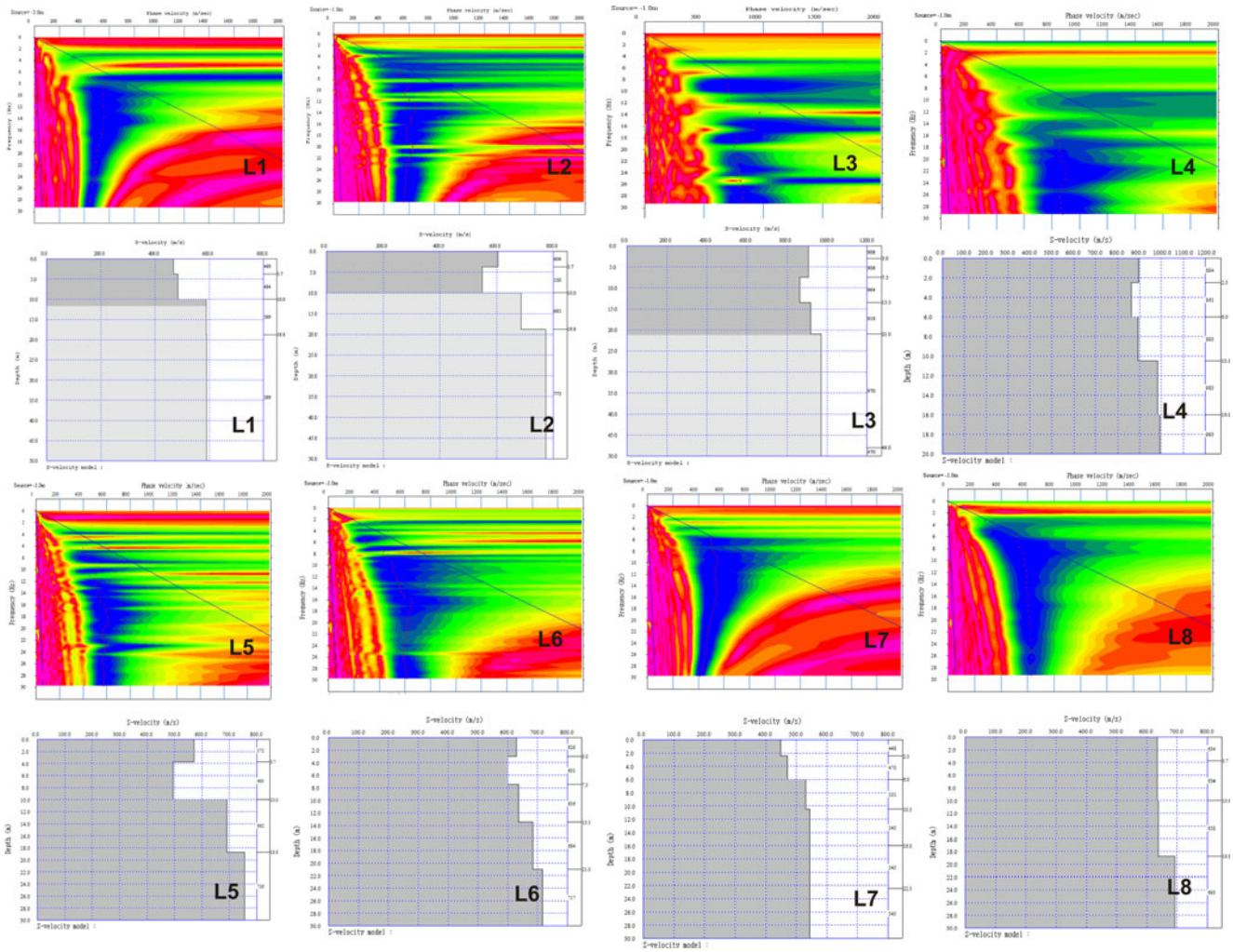

Fig 9 The dispersion curve and the associated S_wave velocity models for whole seismic lines carried out at different parts in Zafarana Wind Farm site. See Fig 1 for the relative position of the conducted seismic lines in this study

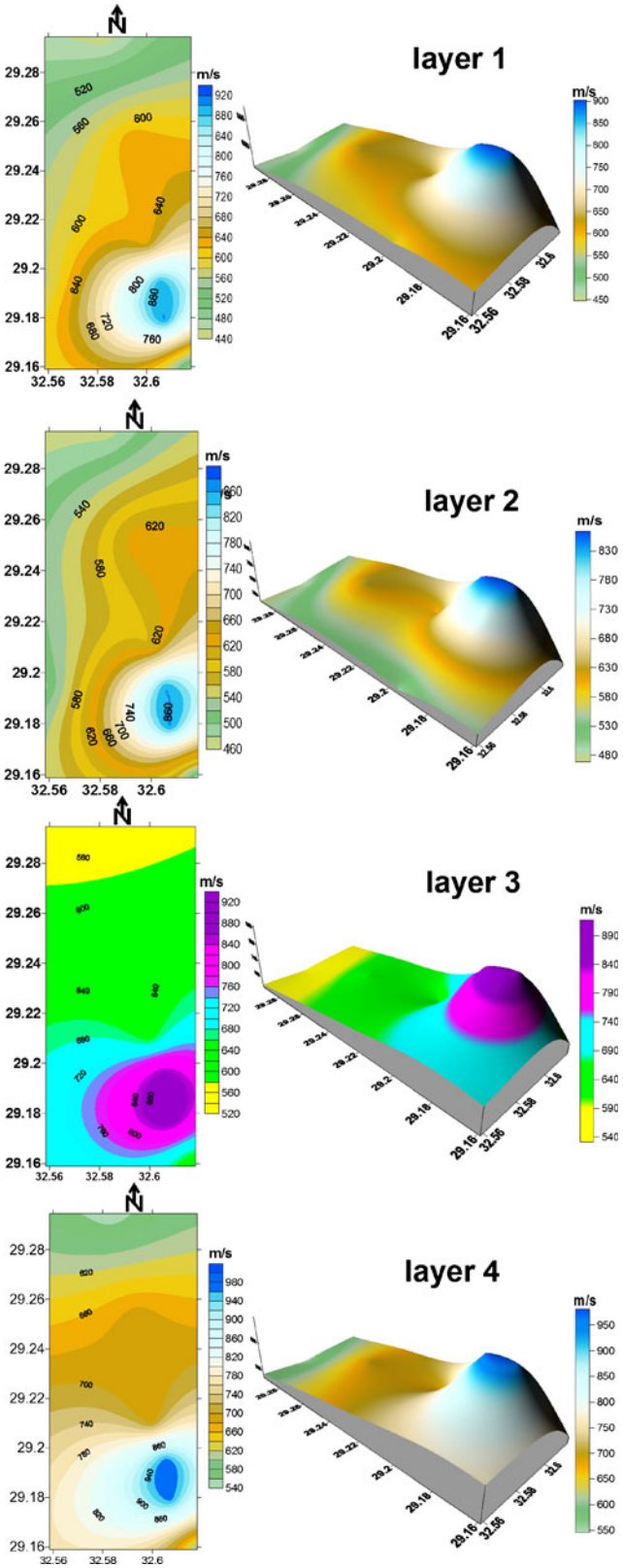

Fig 10 Contour map and 3-D S_wave velocity distribution of the obtained four layers determined from Multi channel Analysis of Surface Wave technique at site of interest

site, while Fig. 8 shows examples of shallow seismic refraction seismograms conducted at the same positions as MASW profiles in order to determine p-wave velocity. Figure 9 shows the dispersion curves and shear wave velocity models of all the conducted seismic lines at Zafarana wind farm.

Deterministic hazard estimation (DSHA)

The seismic hazard in its common form is assigned as any physical phenomenon, such as earthquake ground shaking or ground failure, which is associated with natural or artificial earthquakes and which may produce pernicious effects on buildings and human activities. The seismic hazard approach involves the quantitative estimation of ground-shaking hazards at the site of interest. Seismic hazards may be analysed through one of two principal approaches; deterministic, when a specific earthquake scenario is assumed, or probabilistic, in which uncertainties in earthquake size, location and time of occurrence are taken into account. The difference between deterministic seismic hazard assessment (DSHA) and Probabilistic seismic hazard assessment (PSHA) is that the DSHA design considers only the few (or even only one) earthquakes that are estimated to produce the most severe ground motion at a site. The DSHA method has been outlined by a number of authors (e.g. Abrahamson 2000; Campbell 2005, Deif et al. 2009).

The standard methodology is as follows:

1- determine the seismogenic/seismic zones or zone in and around the site of interest and calculate the maximum magnitude for each seismic source (Table 3)
2- Select the earthquake scenarios (M, R) where M is the magnitude and R is the distance to the site of interest, and calculate the median ground motion for each scenario $(y^{'}|m, r)$
3- Select the largest value of $y^{'}$ $(y_{\max})$ and determine the exceedance probability of

$$y_{\max}: P\,[Y > y_{\max}|m, r].$$

4- Calculate the percentile of *ymax*:

$$X = 1 - P[Y > |m, r] \tag{18}$$

5- Compute the standard normal variate of x (Zx) and calculate at the site of interest the xth percentile value of $y_{\max}$

$$logy_{max,x} = logy_{max} + Z_x \sigma\sigma^a logY \cdot \tag{19}$$

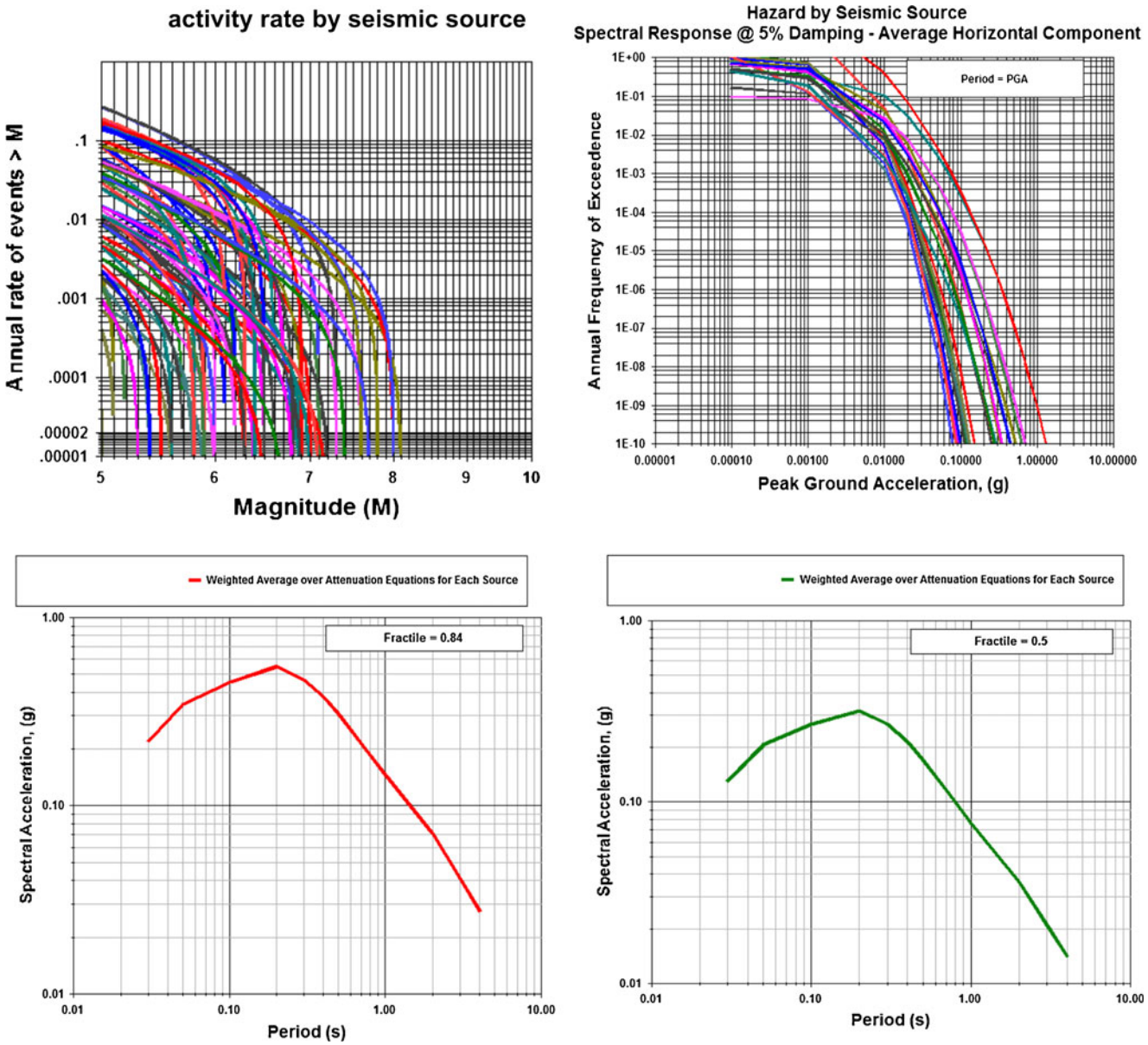

Fig 11 Hazard curves representation at location of seismic line 6 (P6). The left upper panel shows the activity rate for all seismic sources. The right upper panel illustrates the source contribution graphs at PGA period. The left and right lower panels shows the 5 % damping for the median value of horizontal acceleration response spectra at location of seismic profile (P6). The spectrum was calculated over the period range of 0.01–10 s. The ground motion was calculated at 84th, 50th percentile levels for the median peak ground acceleration

The seismic sources, active faults, site effect and subsurface soil characteristics in the investigated area are identified and a maximum magnitude is assigned to each of the seismic sources and faults. The ground motion is then calculated using appropriate attenuation relationships for deterministic analysis. For each calculated maximum magnitude value, the associated strong-motion parameter (acceleration) at the Zafarana wind farm should be estimated using an empirical attenuation relationship. The deterministic approach is essentially based on the worst case scenario, and in case of Zafarana wind farm, a maximum magnitude 6.9 earthquake occurring within an epicentral distance of 17 km with a depth of 15 km will be applied. The effect of this event was calculated at the location of the seismic profile (L6) and is expressed in terms of an acceleration response spectrum, taking into consideration the site effect and soil amplification deduced from Multichannel Analysis of Surface Waves (MASW). Fig. 11 shows the 5 % damping for the median value of horizontal acceleration response spectra at the location of the seismic profile (L6). The spectrum was calculated over the period range of 0.01–10 s. The ground motion was calculated at 50th, 84th percentile levels for the median peak ground acceleration.

Table 3 The identified seismic zones with their main characteristics and recurrence parameters

Zone	M max	M min	Beta	b	Lambda	Averg. Depth	Mmax obs.
1	6.45 + − 0.38	3	2.29 + − 0.17	1.00 + − 0.0	6.919 + − 1.299	14.5	6.2
2	6.55 + − 0.29	3	2.09 + −0.32	0.91 + −0.14	3.051 + − 0.764	15.17	6.3
3	5.55 + − 1.90	3	2.66 + − 0.45	1.16 + − 0.19	1.430 + − 0.405	14.72	5.3
4	5.15 + − 0.44	3	1.15 + − 0.00	0.60 + −0.25	0.605 + − 0.218	14.42	4.9
5	6.25 + − 0.38	3	2.50 + − 0.31	1.09 + − 0.14	2.064 + − 0.565	13.03	6
6	5.3	3	1.55 + − 0.71	0.67 + − 0.31	0.383 + − 0.146	12.52	5.3
7	3.95 + − 0.88	3	3.42 + − 0.00	1.48 + − 0.00	0.337 + − 0.173	14.82	3.7
8	4.40 + − 00	3	3.45 + − 0.00	1.50 + − 0.00		11.28	4.4
9	7.3 + − 0.22	3	1.90 + − 0.13	0.82 + − 0.05	5.569 + − 1.047	15.63	7.2
10	5.25 + − 0.23	3	1.36 + − 0.26	0.59 + − 0.11	2.753 + − 0.641	23.15	5
11	5.65	3	1.15 + − 0.00	0.50 + − 0.00	5.65 + − 2.28	33.27	5.4
12	5.55 + − 0.24	3	1.15 + − 0.00	0.50 + − 0.00	1.294 + − 0.319	25.97	5.3
13	6.15 + − 0.30	3	1.15 + − 0.00	0.50 + − 0.00	6.600 + − 1.786	27.27	5.9
14	5.65 + − 0.50	3	1.15 + − 0.00	0.50 + − 0.00	1.917 + − 0.605	29.33	5.4
15	6.45 + − 0.26	3	1.16 + − 0.00	0.50 + − 0.00	1.611 + − 0.353	25.25	6.2
16	5.65 + − 3.02	3	1.15 + − 0.00	0.50 + − 0.00	0.244 + − 0.131	33	5.4
17	5.35 + − 0.36	3	1.18 + − 0.49	0.51 + − 0.21	0.508 + − 0.182	18.07	5.1
23	6.55 + − 0.68	3	1.25 + − 0.27	0.54 + − 0.12	1.060 + − 0.264	22.64	6.3
24	6.35 + − 0.35	3	1.93 + − 0.26	0.84 + − 0.11	1.561 + − 0.384	26.14	6.1
25	3.95 + − 0.65	3	3.45 + − 0.00	1.50 + − 0.00	0.472 + − 0.226	12.36	3.7
26	6.35	3	1.44 + − 0.43	0.62 + − 0.19	0.569 + − 0.212	26.125	6.1
35	6.35	3	1.30 + − 0.45	0.56 + − 0.19	0.717 + − 0.275	17.59	6.1
36	5.35	3	3.39 + − 0.00	1.47 + − 0.00	2.766 + − 0.672	18.48	5.1
37	5.35 + − 0.45	3	3.45 + − 0.00	1.50 + − 0.00	7.752 + − 1.614	20.76	5.1
38	6.05 + − 00	3	3.45 + − 0.00	1.50 + − 0.00	4.630 + − 0.961	12.08	5.8

Discussion

We conducted a seismic hazard analysis using both the integrated waveform inversion technique and the Multichannel Analysis of Surface Waves (MASW). The seismic hazard assessment in the current study provides a quantitative evaluation of the nature of the ground shaking at the Zafarana wind farm site that might be induced by future maximum earthquakes, taking into consideration the site effect deduced from shallow seismic surveys and associated uncertainness of green function and hazard models. Abd el-aal et al. (2015) conducted probabilistic seismic hazard assessment (PSHA) and stochastic analysis for the site of interest. In their work, they stated that because the hazard was calculated at the bedrock condition they recommended a separate site effect study. This is because the wind farm site is very close to and characterized by soft sediments which can add another seismic hazard dimension due to soil amplification effects.

The application of the moment tensor inversion in this study has yielded a new and significant catalogue of moment tensors for the Gulf of Suez and northern Eastern Desert. The moment tensor catalogue will be useful in future studies on the orientation of the local and regional stress field, for constructing a uniform moment magnitude scale, and for providing constraints on crustal structure and model calibration, as well providing information on the style of deformation and tectonics of the region. By using 3-component broadband seismic waveform data within the local distance recorded by the ENSN, the appropriate velocity model for the ray paths, the moment tensor and the source parameters are mainly determined for three events. More details about waveform inversion procedure steps, station data quality and structure modelling can be found in Abd el-aal and Yagi (2014). The normal faulting obtained from the inversion procedure is consistent with the previous focal mechanism and local stress regime of the area. The obtained results indicate that deformation of the area as a part of the Northern Province of the Eastern Desert and Gulf of Suez is expressed as a crustal extension in the NE-SW direction which is nearly compatible with the horizontal extension direction in the northern part of the Gulf of Suez (Fig 3). This reflects the direct effect of the extensional stress field along the Northern Gulf of Suez spreading centre. Consequently, the obtained source parameters (Tables 1 and 2) are used as input parameters for the hazard source and fault model.

By applying the MASW technique, we obtained the dispersion curves (phase velocity versus frequencies) and by inversion of the dispersion curves, we obtained the shear wave velocity model. Figure 9 shows the dispersion curves and shear wave velocity models of all the seismic lines conducted at Zafarana wind farm. The results reveal that the subsurface layers consist of four to five layers in all the seismic profiles up to a depth of 30 m at the investigated site. The first layer with a thickness of (2.5–7) m is formed from gravels and sands and silty sand (S-wave velocity varies from 450 to 903 m/s). The second layer with a thickness of (3.5 to 8) m is made up of sands and gravels and with less physical properties (S-wave velocity in the range 460 to 860 m/s). The S-wave velocities of the third layer, composed of sandstone, range between 520 and 920 m/s. The S-wave velocities of the fourth layer, composed of claystone, range between 540 and 975 m/s. The fifth layer is exposed only in two sites (at profiles 4 and 6 only) and has S-wave velocities ranging from 700 to 1000 m/s. Figure 10 illustrates the S-wave velocity as obtained from the MASW procedure for each layer. The second layer is characterized by its less physical properties (S-wave velocities). The average shear wave velocity up to 30 m depth, which is known as V_{S30}, was obtained and was used to classify the site according to the International Building Code (IBC-2006). The profiles of p1, p2, p5, p6, P7 and p8 belong to Class C while the profiles p3, p4 belong to Class B.

Conclusion

This study highlights the degree of hazard related to the earthquake activities associated with Zafarana wind farm, in order to predict the possible impact of future damaging earthquakes. For this purpose, we presented and discussed an extended seismic hazard assessment at the site of interest that is based on spectral parameters. The proposed seismic hazard approach includes updating deterministic estimation based on integrated seismic procedures. We have identified the seismic sources that are close enough to the site to give rise to potentially damaging earthquake ground motions. These include distributed sources and active faults which pass through and near the site area. The earthquake loading at the eight individual sites was evaluated using Area and Line Source Models for earthquake sources. In the current approach, we calculated the activity rate from each source. The activity rate graph shows the number of earthquakes vs. their magnitude for all sources in the hazard analysis. This is a standard Richter b-value plot (Fig 11 left upper panel). Where fault activity has been designated by slip rate in mm/year, the slip rate is converted to an activity rate for this plot. Figure 11 (right upper panel) illustrates the source contribution graph. We considered the 50th and 84th percentile, the maximum median ground motion as a reasonable peak ground acceleration because we were using a 'conservative' earthquake magnitude at a closer distance. The provided response spectra, as shown in Fig. 11 (lower panels), reflect the ground shaking at each period. The results obtained in this study with a deterministic approach are compared with the results obtained by the probabilistic method used in Abd el-aal et al. (2014). The differences are mainly related to site effect contributions. In order to provide the engineers and planners responsible for the Zafarana wind farm with complete information on which to base their decisions, the hazard assessment is identified and associated uncertainties are quantified.

Acknowledgments The research was supported by the US-Egypt Cooperative Research Project, entitled: Seismic Risk Assessment of Wind Turbine Towers in Zafarana Wind Farm, Egypt. The authors greatly appreciate the technical staff of seismology department, National Research Institute of Astronomy and Geophysics (NRIAG), for their support in the field measurements. Special thanks to seismologists Rada Sherief and Hazem Badereldein from Egyptian national seismic network.

References

Abd el-aal AK, Kamal H, Abdelhay M, Elzahaby K (2015) Probabilistic and stochastic seismic hazard assessment for wind turbine tower sites in zafarana wind farm, gulf of Suez. Egypt Bull Eng Geol Environ 74:1225–1241. doi:10.1007/s10064-015-0717-x

Abd el-aal AK, Soliman MS (2013) New Sseismic Nnoise Mmodels Obtained Uusing very Bbroadband Sstations. Pure Appl Geophy 170(11):1849–1857. doi:10.1007/s00024-013-0640-7

Abd el-aal AK (2013) Very broadband seismic background noise analysis of permanent good vaulted seismic stations. J Seismolog 17(2):223–237. doi:10.1007/s10950-012-9308-5

Abd el-aal AK (2010a) Modeling of seismic hazard at the northeastern part of greater Cairo metropolitan area. Egypt J Geophys Eng 7(75–90):2010. doi:10.1088/1742-2132/7/1/007

Abd el-aal AK (2010b) Ground motion prediction from nearest seismogenic zones in and around greater Cairo area, Egypt. Nat Hazards Earth Syst Sci 10:1495–1511. doi:10.5194/nhess-10-1495-2010

Abd el-aal AK (2008) Simulating time-histories and pseudo-spectral accelerations from the 1992 Cairo earthquake at the proposed El-Fayoum New City site, Egypt. Acta Geophysica 56:1025–1042. doi:10.2478/s11600-008-0054-6

Abrahamson NA (2000) State of the practice of seismic hazard evaluation. Proc Geo Eng 2000 (Melbourne, Australia) 1:659–685

Aki K (1993) Local site effects on weak and strong ground motion. Tectonophysics 218:93–111

Ambraseys NN, Melville CP, Adams RD (1994) The seismicity of Egypt. Arabia and the Red Sea. Cambridge University Press, Cambridge, p 181

Campbell K (2005) Overview of seismic hazard approaches with emphasis on the management of uncertainties 2nd ICTP workshop on earthquake engineering for nuclear facilities: uncertainties in seismic hazard (Trieste, Italy, 14–25 February 2005)

Deif A, Nofal H, Abou Elenean K (2009) Extended deterministic seismic hazard assessment for the Aswan High Dam, Egypt, with emphasis on associated uncertainty. J Geophys Eng 66:250–263

EGSMA (1983) Geological map of Egypt. Egyptian geological survey and mining authority

Fukao Y, Kikuchi M (1987) Source retrieval for mantel earthquakes by iterative deconvolution of long-period Pwave. Tectonophysics 144: 249–269

Hanks TC, Bakun WH (2002) A bilinear source-scaling model or M-log A observations of continental earthquakes. Bull Seismol Soc Am 92:1841–1846

Hanks TC, Wyss M (1972) The use of body-wave spectra in the determination of seismic-source parameters. Bull Seismol Soc Am 62:561–589

IBC (2006) International Building Code: site classification using the average shear wave velocity in the upper 30 m thickness

Montalvo-Arrieta JC, Sanchez-Sesma FJ, Reinoso E (2002) A virtual reference site for The Valley of Mexico. Bull Seism Soc Am 92: 1847–1854

Maamoun M, Megahed A, Allam A (1984) Seismicity of Egypt. Helwan Institute of Astronomy and Geophysics Bull IV(Ser. B):109–162

Moustafa A, Abd-Allah A (1992) Transfer zones with en echelon faulting at the northern end of the Suez rift. Tectonics 11(3): 499–509

Moustafa A, El-Badrawy R, Gibali H (1998) Pervasive E-ENE oriented faults in Northern Egypt and their effect on the development and inversion of prolific sedimentary basis. Proceedings of 14th petroleum conference, Egyptian General Petroleum Corporation, 1:51–67

Park CB, Miller RD, Xia J (1999) Multichannel analysis of surface waves (MASW). Geophysics 64:800–808

Poirier P, Taher M (1980) Historical seismicity in the near and Middle East, North Africa and Spain from Arabic Documents (VII –XVIII century). Bull Seismol Soc Am 70:2185–2201

Yagi Y, Nishimura N (2011) Moment tensor inversion of near source seismograms. Bulletion of IISEE 45:133–138

Yagi Y, Fukahata Y (2012) Introduction of uncertainty of Green's function into waveform inversion for seismic source processes. Geophys J Int 186(2):711–720

Yagi Y, Nishimura N, Kasahara A (2012) Source process of the May 2008 Wenchuan China, earthquake determined by waveform inversion of teleseismic body waves with a data covariance matrix. Earth Plantes, Space 64:13–16